Depth related variation of isoprenoid and hydroxylated tetraether lipids in Lake Lugu, Southwest China: implications for palaeoenvironmental reconstructions

Jingjing Li [a, *], B. David A. Naafs [b], Rong Wang [a], Xiaoming Lai [c], Hao Long [a], Huan Yang [d], Xiangdong Yang [a]

[a] *State Key Laboratory of Lake Sciences and Environment, Nanjing Institute of Geography and Limnology, Chinese Academy of Sciences, Nanjing 210008, China*

[b] *Organic Geochemistry Unit, School of Chemistry, and School of Earth Sciences, Cabot Institute for the Environment, University of Bristol, Bristol BS8 1TS, UK*

[c] *Key Laboratory of Watershed Geographic Sciences, Nanjing Institute of Geography and Limnology, Chinese Academy of Sciences, Nanjing 210008, China*

[d] *Hubei Key Laboratory of Critical Zone Evolution, School of Geography and Information Engineering, China University of Geosciences, Wuhan 430074, China*

* Corresponding author.

E-mail address: jjli@niglas.ac.cn (J. Li).

ABSTRACT

Archaeal glycerol dibiphytanyl glycerol tetraethers (isoGDGTs) and their hydroxylated derivatives (OH-GDGTs) have been increasingly applied to reconstruct past changes in lake temperature and lake-level using down-core sediments. However, a detailed examination of the distribution pattern of iso- and OH-GDGTs in lacustrine sediments is so far limited. To investigate the controls on the sedimentary GDGT distribution in lakes, we examined the archaeal GDGT distribution in surface sediments at different water depths from Lake Lugu, a deep alpine lake in southwest China. Our aim is to determine their distribution, sources and controlling factors. Based on the significant correlations between iso- and OH-GDGTs in deep-water sediments (> 20 m), we suggest that the main biological source of archaeal GDGTs in surface sediments is aquatic Group I.1a Thaumarchaeota (*Nitrosoarchaeum*). The depth-related variation of iso- and OH-GDGTs indicates that water depth is the main factor affecting the distribution of archaeal GDGTs in Lake Lugu, reflecting that Thaumarchaeota prefer to live in the deeper layer above the oxycline. This relationship leads to a positive correlation between %Cren, %OH-GDGTs, and Cren/Cren' with water depth, confirming their potential application for paleo-lake level reconstruction. Our study improves the understanding of the factors that control the archaeal GDGTs in a deep alpine lake and suggest that they might be used as lake-level indicators.

Keywords: isoGDGTs; OH-GDGTs; water depth; biological sources; lake sediments

1. Introduction

Isoprenoidal glycerol dibiphytanyl glycerol tetraethers (isoGDGTs) are exclusively produced by archaea and characterized by a varying number of cyclopentane moieties [see Schouten et al. (2013) for a review]. The acyclic GDGT-0 is the most common isoGDGT and can be synthesized by all major groups of Archaea, including ammonia-oxidizing Thaumarchaeota, anaerobic methane-oxidizing archaea, methanogens (Pancost et al., 2001; Blaga et al., 2009; Schouten et al., 2013). IsoGDGT with 1 to 3 cyclopentane moieties (GDGT-1 ~ -3) are commonly found in Euryarchaeota, Crenarchaeota and Thaumarchaeota (Schouten et al., 2013), and references therein). A structurally unique GDGT containing 4 cyclopentane moieties and 1 cyclohexane moiety is called crenarchaeol (Sinninghe Damsté et al., 2002), and its isomer (crenarchaeol') is exclusively produced by Thaumarchaeota (Elling et al., 2017; Sinninghe Damsté et al., 2018). In culture experiments there is a correlation between the production of cyclopentane moieties and temperature (De Rosa et al., 1980; Elling et al., 2015). Based on this, the degree of cyclization of isoGDGTs with 1–3 cyclopentane moieties and crenarcheol', expressed as TEX_{86} (TetraEther index of 86 carbon atoms), is proposed to reflect surface temperature in marine environments where the predominant source of isoGDGTs is thaumarchaeota (Schouten et al., 2002). TEX_{86} has also been applied to lacustrine sediments as lake surface temperature proxy (Powers et al., 2010; Tierney et al., 2010a). However, in lacustrine setting, additional sources of isoGDGTs, for example from methanogens, methanotrophs and other non-thaumarchaeotal sources produced either in the surrounding soil, sediment, or water column, could result in unreliable TEX_{86}-inferred temperature in lakes (Blaga et al., 2009; Sinninghe Damsté et al., 2012; Li et al., 2019; Yao et al., 2019).

Besides the regular isoGDGTs, a structurally similar group of archaeal lipids is called hydroxylated GDGTs (OH-GDGTs). They contain 0-2 cyclopentane moieties (OH-GDGT-0, -1, and -2) and have an additional hydroxyl group located in one of the two biphytanyl chains (Liu et al., 2012). OH-GDGTs have been found in marine, lake

and peat environments (Fietz et al., 2013; Wang et al., 2019; Yang et al., 2019; Kou et al., 2022). Thaumarchaeota Group 1.1a are the likely source organisms of OH-GDGTs, while they are absent from Thaumarchaeota Group I.1b which dominate the archaeal community in most soils (Elling et al., 2015; 2017; Bale et al., 2019). Although the physiological function of the additional hydroxy group remains unknown, hydroxylation may result in the enhanced membrane fluidity to maintain the cell membrane properties based on simulations of molecular dynamics (Huguet et al., 2017). This is consistent with the observation of a significant correlation between the sedimentary distribution of OH-GDGTs and sea water temperature at a global scale (Fietz et al., 2013; Huguet et al., 2013; Lü et al., 2015; Yang et al., 2018; Park et al., 2019). While much previous work on OH-GDGTs has focused on marine settings, the distribution of OH-GDGTs in lake environments is scarcely explored (Wang et al., 2019; Kou et al., 2022).

Records of temperature obtained from lacustrine sediment cores based on isoGDGTs have provided promising results within the last decade, these lipids have been increasingly used to reconstruct lake temperatures during the Quaternary (Powers et al., 2011; Blaga et al., 2013; Wang et al., 2015; Morrissey et al., 2018; Sun et al., 2020; Chen et al., 2021). But in addition to temperature, archaeal GDGTs based proxies, such as the fractional abundance of crenarchaeol to total isoGDGTs (%Cren), the ratio of OH-GDGTs to isoGDGTs (%OH-GDGTs), and the ratio of crenarchaeol and crenarchaeol isomer (Cren/Cren') have been proposed as lake-level indicators based on a wide range of lake investigation (Wang et al., 2014a; 2017; 2019; Sun et al., 2020; Kou et al., 2022).

However, before any robust paleolimnological interpretation of such palaeo-proxies in lakes is possible, it is important to develop a comprehensive understanding about the origins of GDGTs and their distribution in modern lacustrine sediments, and within the catchment soils. Multiple studies have evaluated the spatial variation of surface sediments with regard to aspects such as organic carbon (Yu et al., 2015), heavy

metals (Lin et al., 2016) and lipid biomarkers (Sarkar et al., 2014) within a lake basin. The importance of heterogeneity of organic proxies such as *n*-alkanes has been underlined in two lakes from the Tibetan Plateau (Wang et al., 2012b; Kou et al., 2020). However, the basin-scale spatial distribution of GDGTs and their origin within a single lake has been rarely examined so far, limiting the reliable application of GDGTs from a downcore record to reconstruct past environment change. Thus, evaluating the possible spatial variation of GDGTs in modern lake sediments and catchment on a basin scale could reduce the uncertainties in paleoenvironmental reconstructions.

Here we focus on Lake Lugu. It is one of the deepest alpine freshwater lakes in the southeastern margin of the Tibetan Plateau of southwest China (Wang and Dou, 1998). This lake has been considered as an important site for paleolimnological studies due to its sensitivity to changes in the Asian monsoon (Wang et al., 2014b; Sheng et al., 2015; Chang et al., 2018; Zhang et al., 2018). Many studies have showed the significant spatial variability of chironomids (Zhang et al., 2013), diatoms (Wang et al., 2018), trace metals (Lin et al., 2018) and *n*-alkanes (Li et al., 2022) within Lake Lugu. Nevertheless, the spatial distribution pattern of GDGTs and their origin within this lake and catchment are less explored. In order to gain a better understanding of the basin scale heterogeneities and origins of iso- and OH-GDGTs within Lake Lugu, this study mainly focuses on the distribution and origin of archaeal GDGTs from surface sediments with a high spatial resolution. Further, the controlling factor of iso- and OH-GDGTs distribution in Lake Lugu, and the GDGT-based proxy heterogeneities are also discussed for a robust paleolimnological interpretation.

2. Materials and methods

2.1. Study site and sampling

Lake Lugu (27°41′–27°45′N, 100°45′–100°50′E, 2,691 m a.s.l.) is an alpine graben lake that lies at the boundary between Ninglang Yi Autonomous County of Yunnan Province and Yanyuan County of Sichuan Province, the Northwest Yunnan Plateau in

125 southwest China (Fig.1) (NIGLAS, 2019). It is one of the deepest and largest freshwater
126 lakes in China with a maximum water depth of 93.5 m and a mean depth of 40.3 m. The
127 lake has a surface area of 48.45 km^2 and a catchment area of ca. 171.4 km^2 (NIGLAS,
128 2019). It lies within the intermontane basin surrounded by mountains, with Maoniuping
129 Peak situated at 3870 m having the highest altitude in this area (Lin et al., 2000). Lake
130 Lugu is featured by a northwest-southeast direction and divided into two interconnected
131 basins, with a peninsula stretching across its center (Zhang et al., 1997). It is a
132 hydrologically semi-closed lake, which is mainly fed by precipitation, ephemeral runoff,
133 and multiple small rivers and streams (NIGLAS, 2019). Two main inflow tributaries
134 enter the lake. In the east the Shankua River and in the south the Sanjiacun River. There
135 is one outflow through the Gaizu River in the southeast that drains the lake via the
136 Caohai wetland into the Yalong River, a tributary of the Yangtze River (Yang, 1984).
137 Lake Lugu is an oligotrophic (TP and TN, 12.7 and 107.9 $\mu g \cdot l^{-1}$) and warm temperate
138 monomictic lake, with thermal stratification typically beginning in early April and
139 strong stratification during summer and early autumn. While in early winter the
140 thermocline breaks down and water column mixing occurs in late winter to early spring
141 (Wen, 2017; Wang et al., 2018).
142 The climate of this region is mainly determined by Indian summer monsoon in
143 summer and the southern branch of the westerlies in winter, leading to a temperate
144 climate with distinct dry and wet seasons: approximately 90% of the annual
145 precipitation (~940 mm) occurs between May and October (Wang et al., 2014b; 2018).
146 The mean annual air temperature is ca. 12.8 °C; the mean monthly minimum and
147 maximum temperatures are in December and July (5.6, 19.4 °C, respectively). The
148 terrestrial vegetation in the catchment features a strong altitudinal gradient. Overall, the
149 major plant taxa consist of a mixture of *Acer davidii*, *Populus davidiana* and *Pinus*
150 *yunnanensis* (Li et al., 2013). Submersed macrophytes are mainly distributed in shallow
151 water (<10 m) and are composed of *Ottelia acuminate*, *Potamogeton pectinatus*, and
152 *Potamogeton tepperi* (Tan and Dong, 2011). The main emersed aquatic plants are

153 composed of *Phragmites australis*, *Zizania caduciflora*, *Typha orientalis*, and *Scirpus*
154 *Validus* (Zhao et al., 2016). The predominant soil type in lake catchment consists out of
155 brunisolic soil, red loam, yellow brown soil, purple soil and limestone soil (Zhang et
156 al., 1997).

157 Lake surface sediments at different water depths and mineral soils from the
158 catchment area were obtained during two field campaigns in 2012 and 2015. The
159 locations of the sampling sites are shown in Fig. 1 (For coordinates and water depths,
160 see Supplementary Table S1). 54 lake surface sediments (0–2 cm) were collected using
161 a stainless steel box corer. Nine topsoils (upper 0–2 cm) from within the catchment
162 were also sampled. Surface sediment and soil samples were freeze-dried and ground to
163 powder to homogenize after transport to the laboratory.

164

165 *2.2. Lipid extraction and GDGT analysis*

166 All samples were ultrasonically extracted as previously described in Li et al.
167 (2022). Briefly, the freeze-dried sample (ca. 5 g dry weight) was extracted four times
168 by ultrasonication using a mixture of dichloromethane and methanol (9:1, v/v). The
169 total lipid extract was subsequently saponified with 6% KOH in methanol. The neutral
170 lipids were extracted with hexane and then separated by column chromatography with
171 activated silica gel as the stationary phase by using hexane and methanol to obtain the
172 apolar and polar fractions, respectively. The polar fraction containing iso- and OH-
173 GDGTs was filtered over a 0.45μm polytetrafluoroethylene (PTFE) filter with
174 hexane/isopropanol (99:1, v/v), and was then dried under gentle stream of N_2 gas prior
175 to further analysis.

176 The archaeal GDGTs were analysed using high performance liquid
177 chromatography-positive ion atmospheric pressure chemical ionization with triple
178 quadrupole mass spectrometry (HPLC-APCI-MS) on an Agilent 1200 series (USA).
179 Analytical separation of GDGTs was achieved using two silica columns in tandem (150
180 mm × 2.1 mm, 1.9 μm; Thermo Finnigan) following the method of Yang et al. (2015).

The solvent program started with isocratically eluting for the first 5 min with 84% A and 16% B, where A = *n*-hexane and B = EtOAc. This was followed by an elution gradient that consisted out of: 84/16 A/B to 82/18 A/B from 5–65 min and then to 100% B in 21 min, followed by 100% B for 4 min to wash column and then back to 84/16 A/B to equilibrate the column for 30 min at a constant rate of 0.2 ml/min throughout. Selected ion monitoring (SIM) mode was used to increase sensitivity and reproducibility, with *m/z* 1318, 1316, 1314, 1300, 1298 and 1296 as the targeted $[M+H-18]^+$ and $[M+H]^+$ ions for detection of OH-GDGTs, while *m/z* 1302, 1300, 1298, 1296, 1292, 1050, 1048, 1046, 1036, 1034, 1032, 1022, 1020 and 1018 for isoGDGTs and brGDGTs, respectively. Concentrations were determined by integration of peak areas of the $[M+H]^+$ ions of C_{46} GTGT internal standard (*m/z* 744, concentration of 11.57 ng/µl) (Huguet et al., 2006) and GDGTs of interest, and then normalized to dry weight (dw). Quantification was semi-quantitative as the relative response factors between GDGTs and standard were not determined.

2.3. GDGTs-based proxy calculations

Fractional abundances of individual isoGDGT were expressed as the fractional abundances of the total isoGDGTs, i.e., the sum of crenarchaeol (Cren) and its isomer (Cren'), GDGT-0, -1, -2, and -3.

The TEX_{86} reflects the degree of cyclization of particular isoGDGTs and was calculated according to Schouten et al. (2002):

$$TEX_{86} = \frac{([GDGT-2]+[GDGT-3]+[Cren'])}{([GDGT-1]+[GDGT-2]+[GDGT-3]+[Cren'])} \quad (1)$$

The branched versus isoprenoid tetraether (BIT) index was calculated following Hopmans et al. (2004), reflecting the relative abundance of bacterial brGDGTs vs. archaeal crenarchaeol.

$$BIT = \frac{([Ia]+[IIa]+[IIIa]+[IIa']+[IIIa'])}{([Ia]+[IIa]+[IIIa]+[IIa']+[IIIa']+[Cren])} \quad (2)$$

The Methane Index (MI) is expressed as the degree of cyclic GDGT-1, -2 and -3

to crenarchaeol and its isomer and was calculated according to Zhang et al. (2011):

$$MI = \frac{([GDGT-1]+[GDGT-2]+[GDGT-3])}{([GDGT-1]+[GDGT-2]+[GDGT-3]+[Cren]+[Cren'])} \quad (3)$$

The Ring Index (RI) represents the weighted average number of cyclopentane rings and was calculated according to Zhang et al. (2016):

$$RI = \frac{(0\times[GDGT-0]+1\times[GDGT-1]+2\times[GDGT-2]+3\times[GDGT-3]+4\times[Cren]+4\times[Cren'])}{([GDGT-0]+[GDGT-1]+[GDGT-2]+[GDGT-3]+[Cren]+[Cren'])} \quad (4)$$

The $R_{i/b}$ (Xie et al., 2012) represents the relative abundance of total isoGDGTs to total brGDGTs:

$$R_{i/b} = \sum isoGDGTs / \sum brGDGTs \quad (5)$$

The relative abundance of crenarchaeol and its isomer is calculated according to Li et al. (2016):

$$Cren/Cren' = crenarchaeol / crenarchaeol' \quad (6)$$

Fractional abundances of individual OH-GDGTs were calculated as the fractional abundances of the total OH-GDGTs, i.e., the sum of OH-GDGT-0, -1 and -2. The %OH-GDGTs is calculated following Fietz et al. (2013):

$$\%OH-GDGTs = \frac{\sum OH-GDGTs}{\sum OH-GDGTs + \sum isoGDGTs} \quad (7)$$

The ring index of OH-GDGTs (RI-OH) represents the weighted average number of cyclopentane moieties and is calculated according to Lü et al. (2015). The revised ring index of OH-GDGTs (RI-OH') is also calculated according to Lü et al. (2015).

$$RI-OH = \frac{([OH-GDGT-1]+2\times[OH-GDGT-2])}{([OH-GDGT-1]+[OH-GDGT-2])} \quad (8)$$

$$RI-OH' = \frac{([OH-GDGT-1]+2\times[OH-GDGT-2])}{([OH-GDGT-0]+[OH-GDGT-1]+[OH-GDGT-2])} \quad (9)$$

2.4. Statistical analysis

Principal component analysis (PCA) was performed on the fractional abundances of archaeal GDGTs to provide a view of the variability within the iso- and OH-GDGTs in Lake Lugu using CANOCO version 5. Redundancy analysis (RDA) of archaeal GDGTs and related proxies in surface sediments were performed to analyse their

234 relationship with water depth. The spatial distribution of iso- and OH-GDGTs in surface
235 sediments was performed using ArcGIS 10.6 software, with the kriging method of
236 gridding applied for data interpolation. The independent sample *t*-test was performed
237 using SPSS software to discriminate the significance of differences in concentration of
238 iso- and OH-GDGTs in surface sediments at different water depths.
239
240 **3. RESULTS**
241 *3.1. Distribution of iso- and OH-GDGTs in surface sediments and soils*
242 All isoGDGTs (GDGT-0 to -3, crenarchaeol and its isomer, Cren') were detected
243 in the lake surface sediments. However, concentrations were highly variable with three
244 order of magnitude differences, ranging from 8 to 7370 ng g^{-1} dw, with an average of
245 1360 ng g^{-1} dw (Table S1). The summed concentration of isoGDGTs was lowest in
246 the surrounding mineral soils with values from 1 to 120 ng g^{-1} dw (average of 20 ng
247 g^{-1} dw) (Table S1). The isoGDGT-0 and crenarchaeol were the two most abundant
248 compounds across all sample types (Fig. 2a). Although the average fractional
249 abundances of GDGT-0 and crenarchaeol in surface sediments were similar (avg. 42
250 and 41%), GDGT-0 had a wider range than crenarchaeol. By contrast, the average
251 fractional abundance of crenarchaeol (41%) was higher than GDGT-0 in soils (36%)
252 (Fig. 2a). The fractional abundance of GDGT-1 to -3 was low in lake surface sediments
253 and soils, with an average of 17% and 18%, respectively. The TEX_{86} and BIT values
254 of soils (0.89 ± 0.06, 0.94 ± 0.07) were higher than surface sediments (0.81 ± 0.08,
255 0.74 ± 0.15) (Fig. 3 and Table S1). However, the $R_{i/b}$ value of surface sediments was
256 much higher than soils, with an average of 0.7 and 0.1, respectively.
257 OH-GDGTs were detected in 51 of the 54 lake surface sediment samples. The three
258 exceptions were LG-1, -2 and -5, all with a shallow water depth of < 3 m (Table S1).
259 The summed concentration of OH-GDGTs ranged from 2 to 1050 ng g^{-1} dw, with an
260 average of 160 ng g^{-1} dw (Table S1). The average fractional abundance of OH-GDGT-
261 0 was higher (40%) than OH-GDGT-1 (27%) and OH-GDGT-2 (34%) (Fig. 2b). The

RI-OH value of surface sediments was 1.56 ± 0.09. The concentration of OH-GDGTs in surrounding soils was below the detection limit (Fig. 2b).

3.2. Statistical analysis of iso- and OH-GDGT distributions in surface sediments

The first two components explain a cumulative 92% of the variance in the PCA (Fig. 2c). On the first principal component (PC1, explaining 84% of the variance) the loading of GDGT-0 is opposite to that of all other isoGDGTs. GDGT-1 and -2 are negatively loaded with the second principal component (PC2, explaining ~8% of the variance), while GDGT-3, crenarchaeol and its isomer are in the same quadrant in the PCA biplot (Fig.2c). RDA analysis of the fractional abundance of isoGDGTs and proxies was performed to analyse the relationship among TEX_{86}, BIT, RI, MI, and water depth (Fig.2d). Like the PCA result, GDGT-0 is positively loaded on the first axis of RDA (RDA1, explaining 79% of the variance), and has an opposite loading to the other isoGDGTs (Fig.2d). The RDA2 explains 6% of the variance. Crenarchaeol is negatively loaded on the RDA2, while GDGT-2, -3, and crenarchaeol' are positively loaded on RDA2 (Fig.2d). The RDA analysis further highlights the negative correlation between GDGT-0 and water depth, while other isoGDGTs are positively correlated with water depth (Fig.2d). The average values of GDGT-0/Cren exhibit the following profile: shallow-water sediments (51) > soils (1.7) > deep-water sediments (0.6) (Fig. 3e and Table S1).

The PCA and RDA results can be verified by the distribution pattern of isoGDGTs in surface sediments. The isoGDGTs in shallow lake sediments (water depth < 20 m, n = 14) are dominated by GDGT-0, which constitute ~80% of the total isoGDGTs (Fig.2a and Table S1). However, crenarchaeol is the main component in deep sediments (water depth > 20 m, n = 40), with an average of 51% (Fig.2a and Table S1).

The PCA and RDA results of OH-GDGTs suggest that OH-GDGTs are less affected by water depth compared to isoGDGTs (Figs.2e and f). This can be verified by the distribution pattern of OH-GDGTs in surface sediments (Fig. 2b and Table S1). For

example, OH-GDGT-0 is dominant in both in shallow (< 20 m) and deep (> 20 m) sediments, with the average of 42 ± 11% and 39 ± 3%, respectively. Similarly, OH-GDGT-2 (average, ~ 35%) is higher than OH-GDGT-1 (average, ~ 25%) in shallow and deep sediments (Fig. 2b).

The different archaeal GDGT distributions between shallow and deep sediments is also seen in their related proxies, such as BIT, RI and Cren /Cren' (Fig. 3). However, OH-GDGT based proxies such as RI-OH and RI-OH' show no substantially difference, as only %OH-GDGTs differ between shallow and deep sediments (Fig. 3h).

4. DISCUSSION

4.1. Potential sources of iso- and OH-GDGTs in surface sediments

4.1.1. isoGDGTs

The average summed concentration of isoGDGTs in lake surface sediments is much higher than that of soils (Table S1). The substantial discrepancy in concentration between sediments and soils can be explained by *in situ* production of isoGDGTs within the lake. This is further supported by the observation that the different isoGDGT-based proxies are different in lake sediment samples compared to mineral soils (Fig. 3). For example, soils have a higher TEX_{86} and BIT values than lake sediments (Figs. 3b and c), whereas lake sediments exhibit higher GDGT-2/GDGT-3 and Cren/Cren' ratios compared to soils (Figs. 3f and g), all of which demonstrated by an independent sample *t*-test with $p < 0.05$. Our finding of *in situ* production within this large lake system is consistent with previous studies (Li et al., 2019; Wang et al., 2019; Yao et al., 2019; Baxter et al., 2021; Kou et al., 2022; Sinninghe Damsté et al., 2022). Moreover, the depth related variation in isoGDGTs indicates that there is a deep-water contribution of crenarchaeol. The relative low concentration of oxygen in the deeper and colder (suboxic) part of the lake likely provides a niche for nitrifying thaumarchaea (Könneke et al., 2005; Wuchter et al., 2006; Qin et al., 2017), allowing the proliferation of Thaumarchaeota as seen in other lakes (Baxter et al., 2021; Sinninghe Damsté et al.,

318 2022). More details of depth related variation of isoGDGTs distribution are discussed
319 in Section 4.2.
320 The ratio of isoGDGT-0 over crenarchaeol (GDGT-0/Cren) has been used to infer
321 the relative contribution of methanogenic archaea producing isoGDGTs within lakes
322 with values >2 indicative of a significant methanogen contribution (Blaga et al., 2009;
323 Li et al., 2019). The high values of GDGT-0/Cren in shallow-water sediments (average
324 ~40) thus indicates a dominant contribution of methanogens to the sedimentary
325 isoGDGT pool (Fig. 3e). This methanogen input is unlikely to be derived from soils in
326 the catchment area as the ratio is much lower (average <1) in mineral soils, indicative
327 of a major contribution of Thaumarchaeota (Fig. 3e). Similarly low ratios are found in
328 deep-water sediments, implying a major contribution of Thaumarchaeota and a minor
329 contribution of methanogens in the deeper part of the lake (Fig. 3e). The concentrations
330 of GDGT-0 and crenarchaeol are not correlated in shallow-water sediments ($R^2 = 0.01$,
331 $p < 0.05$, n = 14) (Fig. 4f), but do exhibit a significant linear correlation ($R^2 = 0.98$, $p <$
332 0.05, n = 40) in deep-water sediments. This result strongly suggests that contribution to
333 the isoGDGT pool between shallow- and deep-water sediments is different.
334 The ratio of crenarchaeol over its isomer (Cren/Cren') has been used to
335 differentiate between Group I.1a versus I.1b Thaumarchaeota as they produce
336 crenarchaeol and crenarchaeol' in varying proportions. High ratios of Cren/Cren' (>25)
337 are indicative for the Group I.1a Thaumarchaeota, while a lower ratio (<25) is
338 indicative for Group I.1b Thaumarchaeota (Li et al., 2016; Kou et al., 2022). Both the
339 average Cren/Cren' values of shallow- and deep-water sediments (averages of 41 and
340 74) are higher than soils (9) (Fig. 3g). This suggests the dominance of aquatic Group
341 I.1a Thaumarchaeota in lake sediments, while Group I.1b Thaumarchaeota are
342 abundant in soils and further demonstrates that the contribution from isoGDGTs
343 produced in the catchment soils to the lake sediments is small.
344 Recently, analysis of metagenome-assembled genomes (MAGs) of
345 Thaumarchaeota (now referred as the class *Nitrososphaeria* in the phylum

346 *Thermoproteota*, Rinke et al. (2021)) was performed on surface sediments along a water
347 depth gradient in Lake Lugu. It revealed that the dominant thaumarchaeal OTU was
348 *Nitrosoarchaeum* (Ren and Wang, 2022). Additionally, the archaeal 16S rRNA gene
349 amplicon data clarified the depth variation of *Nitrosoarchaeum* (affiliated to Group I.1a)
350 abundance, with a peak ranging from 20 to 50 m depth around the thermocline zone,
351 showing less variations toward shallow layers above 20 m and deep layers below 50 m
352 (Ren and Wang, 2022). This depth variation of *Nitrosoarchaeum* is consist with the
353 concentration profile of isoGDGTs in surface sediments along our water depth gradient,
354 with the highest concentration at ~ 50 m (Fig. S1a–g). This finding confirms the
355 biological source of isoGDGTs in Lake Lugu to be predominantly Thaumarchaeota
356 (*Nitrososphaeria*). These results consist with previous studies in deep oligotrophic
357 lakes where *Nitrosoarchaeum* is the dominant thaumarchaeal OTU (Hiraoka et al., 2019;
358 Podowski et al., 2022), while in other lakes *Nitrosopumilus* is the main thaumarchaeal
359 OTU (Herber et al., 2020; Klotz et al., 2022; Sinninghe Damsté et al., 2022). This
360 discrepancy may be due to the varying climate and environmental conditions in
361 different regions.
362
363 *4.1.2. OH-GDGTs*
364 OH-GDGTs have been reported in the cultures of Nitrosopumilales, such as the
365 *Nitrosopumilus* and *Nitrosoarchaeum* clades, which are attributed to Group I.1a
366 Thaumarchaeota (Elling et al., 2017; Bale et al., 2019). However, the Nitrososphaerales
367 (Group I.1b Thaumarchaeota) which are typically the dominant Thaumarchaeota in
368 mineral soils do not produce OH-GDGTs (Elling et al., 2017; Bale et al., 2019). In Lake
369 Lugu, OH-GDGTs are only detected in lake surface sediments and not in the soils from
370 the catchment, indicating that these lipids must be produced *in situ* within the lake. This
371 is consistent with our finding of higher concentrations of summed and individual OH-
372 GDGTs in deep-water sediments compared to shallow-water sediments (Fig. S1h–k).
373 This result is consist with previous findings of OH-GDGTs reported in mid-latitude

374 Asia, Tibetan Plateau and central European lakes (Wang et al., 2019; Kou et al., 2022;
375 Sinninghe Damsté et al., 2022).

376 The biological source of OH-GDGTs in deep-water sediments might be similar to
377 that of the isoGDGTs, as there is a high correlation between the concentrations of both
378 lipid classes ($R^2 = 0.98$, $p < 0.05$, $n = 40$) (Fig. 4f). Moreover, the concentration profiles
379 of the total and individual OH-GDGTs all correlate well with those of GDGT-0 (avg.
380 $R^2 = 0.96$) and crenarchaeol (avg. $R^2 = 0.99$) in deep-water sediments (Figs. 4g, h and
381 S2), strongly suggesting that OH-GDGTs are also sourced from Thaumarchaeota, likely
382 predominantly *Nitrosoarchaeum* (Ren and Wang, 2022). However, there is no strong
383 relationship between OH-GDGTs and isoGDGTs such as GDGT-0 and crenarchaeol in
384 shallow-water sediments (Figs. 4g, h and S2). Only OH-GDGT-0 is moderately
385 correlated ($R^2 = 0.31$, $p < 0.05$, $n = 14$) to GDGT-0, indicating that OH-GDGT-0 might
386 have a (partial) methanogens origin. No correlation between the concentrations of OH-
387 GDGT-0 and crenarchaeol ($R^2 = 0.18$, $p < 0.05$, $n = 14$) also implies that thaumarchaeota
388 are unlikely a major source for OH-GDGT-0 in shallow-water sediments (Fig. S2b).
389 Notably, the concentrations of OH-GDGT-2 and crenarchaeol are strongly correlated
390 ($R^2 = 0.89$, Fig. S2f) in shallow-water sediments, suggesting they may share a similar
391 biological source of *Nitrosoarchaeum* (Ren and Wang, 2022).

392 In summary, the difference in two depth profiles of OH-GDGTs is most likely due
393 to their different sources in shallow- and deep-water sediments. The identical
394 relationship between crenarchaeol and OH-GDGTs in deep-water sediments can be
395 interpreted as their similar biological source, i.e., *Nitrosoarchaeum*, while a
396 contribution of methanogens for OH-GDGT-0 cannot be excluded in shallow-water
397 sediments.

398

399 *4.2. Depth-related variation of iso- and OH-GDGTs in surface sediments*

400 The isoGDGTs in surface sediments of Lake Lugu are predominantly produced *in*
401 *situ* within the lake and their relative abundances and concentrations are strongly

affected by water depth (Figs. S1 and S3). The RDA analysis indicates that water depth is an important factor influencing lake sedimentary isoGDGTs distribution (Fig. 2d). GDGT-0 and crenarchaeol are the two main components of isoGDGTs in sediments with regards to shallow- and deep-waters (Fig. 2), their fractional abundances are both well correlated with water depth (R^2 = 0.75 and 0.7, respectively, n = 54) (Figs. 4a and b). Moreover, the relative abundances of other isoGDGTs also exhibit strong/moderate relationships with water depth (GDGT-1, -2, and crenarchaeol', with the R^2 of 0.77, 0.56 and 0.4, Fig. S3). Thus, our results collectively demonstrate that the isoGDGT distribution in surface sediments of Lake Lugu is primarily controlled by water depth. Although the RDA result indicates that the correlation between OH-GDGTs and water depth is not as strong as that of isoGDGTs (Fig. 2f), their distribution in surface sediments is also associated with water depth. It should be noted that the %OH-GDGTs is significantly correlated with water depth (R^2 = 0.7, $p < 0.05$, n = 54) (Fig. 4d). As the OH-GDGTs and crenarchaeol are suggested to share similar biological source of *Nitrosoarchaeum* in deep-water sediments (Section 4.1), their strong positive correlation with water depth can be interpreted as a common ecological response of *Nitrosoarchaeum* to water depth in lake environments.

Lugu Lake is characterized by substantially enhanced concentrations of iso- and OH-GDGTs in deep-water sediments compared to shallow-water sediments (Fig. S1). The depth-related variations of iso- and OH-GDGTs in surface sediments is confirmed in their interpolated spatial distribution of related proxies (Fig. 5). Crenarchaeol is the most abundant isoGDGTs in deep-water sediments and its average concentration is several orders of magnitude higher (860 ng g^{-1} dw) than that of shallow-water sediments (20 ng g^{-1} dw) (Fig. S1 and Table S1). Thus, low BIT values in deep-water sediments can be explained by the depth-dependent variation of crenarchaeol with increased production in the deeper lake water (Figs. 5d and 4c). Thaumarchaeota are prone to thrive in deep water above the oxycline of deep lakes (Buckles et al., 2013; Baxter et al., 2021; Sinninghe Damsté et al., 2022). In Lake Lugu, the proper niche for

Nitrosoarchaeum to proliferate is between 20–50 m depth (Ren and Wang, 2022). This control is different from that found for other lipid classes.

A depth variation in crenarchaeol abundance in surface sediments has also been observed in lakes from East Africa, midlatitude Asia, and the Tibetan Plateau (Tierney et al., 2010b; Wang et al., 2019; Kou et al., 2022). Based on the significant strong correlation between crenachaeol and water depth, the ratio of crenarchaeol to total isoGDGTs (%Cren) has been proposed as an indicator for lake level and has been used to reconstruct past changes in lake levels (Wang et al., 2014a; 2017). Recently, %OH-GDGTs (the ratio of total OH-GDGTs to total isoGDGTs) (Wang et al., 2019), and the Cren/Cren' have been applied to reflect the lake level change as well (Sun et al., 2020; Kou et al., 2022). However, the correlations between GDGT-based indices and water depth in these previous studies are weaker compared to our dataset. For example, the correlation coefficient (R^2) between water depth and %Cren in Lake Lugu is 0.77 (n = 54) (Fig. 4b), however, the correlation coefficient decreases to 0.46 when the dataset (n = 227) of all available midlatitude Asia and Tibetan Plateau lakes was added (Fig. 6a). Similar variations have been observed between the relationship of %OH-GDGTs, Cren/Cren' and water depth. They exhibit moderate (R^2 = 0.55) and low (R^2 = 0.47) correlations with water depth when previous reported lake datasets are added (Figs. 6b and c). It is likely that on a global scale other potential influencing factors such as temperature, pH, nutrient status, and salinity affect these relationships.

The significant strong correlation between BIT and water depth (R^2 = 0.71) in Lake Lugu (Fig. 4c), is also consistent with previous findings. Similar relationships have been observed in 82 lakes from a global database (Blaga et al., 2010), as well as in East African lakes (Tierney et al., 2010b), Chilean lakes (Kaiser et al., 2015), Tibetan Plateau lakes (Wang et al., 2012a; 2016; Kou et al., 2022) and midlatitude Asian lakes (Wang et al., 2019). Although the correlation between BIT and water depth (R^2 = 0.31, p < 0.05, n = 227) is not as strong as Lake Lugu when all lakes are integrated, the BIT exhibits a negatively relationship with water depth in most lakes (Fig. 6d). This relationship is

458 probably due to the preferred habitat for Thaumarchaeota in deeper waters.

459

460 *4.3. Implications for paleolimnological studies*

461 Iso- and OH-GDGT based proxies, i.e., %Cren, %OH-GDGTs and Cren/Cren'
462 have been used to reconstruct lake water level from ancient and modern lake sediments
463 (Wang et al., 2017; 2019; Sun et al., 2020; Wu et al., 2020; Chen et al., 2021). In Lake
464 Lugu, these archaeal GDGTs also correlate well with water depth and can serve as the
465 indicator of lake level. However, a prerequisite for applying these archaeal GDGT
466 indicators is to ascertain that nitrifying Thaumarchaeota could thrive under certain lake
467 condition, such as the larger and deeper lakes. Thus, the oligotrophic/mesotrophic lakes
468 with sufficient oxygen for ammonia oxidation do offer a proper niche for the nitrifying
469 thaumarchaea such as *Nitrosopumilale* and *Nitrosoarchaeum*, and subsequently leading
470 to the high production of crenarchaeol. In contrast, small and shallow lakes that are
471 prone to be affected by eutrophication, which favor high production of GDGT-0 but
472 minor crenarchaeol or OH-GDGTs, limiting the application of archaeal GDGTs as lake-
473 level indicator.

474 The spatial distribution of iso- and OH-GDGTs in Lake Lugu have showed that
475 water depth is the main factor for their distribution, which is different from the spatial
476 heterogeneity of *n*-alkanes that are mainly affected by soil erosion in this lake (Li et al.,
477 2022). The depth variation of archaeal GDGTs in Lake Lugu revealed that the fractional
478 abundances of iso- and OH-GDGTs remain constant between the depth range of 40–60
479 m (Figs. 4 and S3). For example, %Cren reached the maximum (~ 60) at the water depth
480 of 40 m and show less variability at the depth range < 60 m (Fig. 6a). Similar
481 distribution pattern of %Cren is also observed in mid-altitude Asian and Tibetan Plateau
482 lakes (Wang et al., 2019; Kou et al., 2022), the %Cren all remain unchanged at the water
483 depth > 40 m (Fig. 6a). This likely reflects the physiology of Thaumarchaeota in lake
484 environments, which prefer to live in the deep layer of lake with oxygen.

485

5. CONCLUSIONS

We examined the distribution of iso- and OH-GDGTs in surface sediments from different water depths of Lake Lugu as well as mineral soils from the catchment to determine their sources and factors that impact their distributions. Different isoGDGTs distribution between mineral soils and lake surface sediments indicates that isoGDGTs in lake sediments are mainly produced within the lake, while the terrestrial contribution is minor. The biological source of crenarcheaol in lake sediments is probably *Nitrosoarchaeum*, the dominant thaumarchaeal OTU based on a previous molecular biological study. Our data show that water depth is the main factor affecting the archaeal GDGT distribution in Lake Lugu. Both the %Cren and %OH-GDGTs of surface sediments are correlated with water depth, suggesting that they could be used as proxies for past lake-level changes.

ACKNOWLEDGEMENTS

Two anonymous reviewers and the editor are thanked for their constructive comments. We would like to thank S. Zhao for LC-MS maintenance. We thank Drs. H. Wang and Q. Kou for providing their lake data. Dr. H. Sun is thanked for composing figures. J.L. was funded by the National Natural Science Foundation of China (41977384), Science and Technology Planning Project of Nanjing Institute of Geography and Limnology, Chinese Academy of Sciences (NIGLAS2022TJ04) and the Open Foundation of Hubei Key Laboratory of Critical Zone Evolution, China University of Geosciences (CZE2022F01). R.W. acknowledges the financial supports of the Youth Scientists Group in Nanjing Institute of Geography and Limnology, Chinese Academy of Sciences (2021NIGLAS-CJH03). B.D.A.N. acknowledges a Royal Society Tata University Research Fellowship for funding.

REFERENCES

Bale, N.J. et al., 2019. Membrane lipid composition of the moderately Thermophilic ammonia-oxidizing archaeon "Candidatus *Nitrosotenuis uzonensis*" at different growth temperatures. Applied and Environmental Microbiology, 85(20): e01332-19.

Baxter, A.J. et al., 2021. Seasonal and multi-annual variation in the abundance of isoprenoid GDGT membrane lipids and their producers in the water column of a meromictic equatorial crater lake (Lake Chala, East Africa). Quaternary Science Reviews, 273: 107263.

Blaga, C.I., Reichart, G.-J., Heiri, O., Sinninghe Damsté, J.S., 2009. Tetraether membrane lipid distributions in water-column particulate matter and sediments: a study of 47 European lakes along a north–south transect. Journal of Paleolimnology, 41(3): 523-540.

Blaga, C.I., Reichart, G.-J., Lotter, A.F., Anselmetti, F.S., Sinninghe Damsté, J.S., 2013. A TEX_{86} lake record suggests simultaneous shifts in temperature in Central Europe and Greenland during the last deglaciation. Geophysical Research Letters, 40(5): 948-953.

Blaga, C.I. et al., 2010. Branched glycerol dialkyl glycerol tetraethers in lake sediments: Can they be used as temperature and pH proxies? Organic Geochemistry, 41(11): 1225-1234.

Buckles, L.K., Villanueva, L., Weijers, J.W.H., Verschuren, D., Sinninghe Damsté, J.S., 2013. Linking isoprenoidal GDGT membrane lipid distributions with gene abundances of ammonia-oxidizing *Thaumarchaeota* and uncultured crenarchaeotal groups in the water column of a tropical lake (Lake Challa, East Africa). Environmental Microbiology, 15(9): 2445-2462.

Chang, J. et al., 2018. A 2500-year climate and environmental record inferred from subfossil chironomids from Lugu Lake, southwestern China. Hydrobiologia, 811(1): 193-206.

Chen, L. et al., 2021. GDGTs-based quantitative reconstruction of water level changes and precipitation at Daye Lake, Qinling Mountains (central-east China), over the past 2000 years. Quaternary Science Reviews, 267: 107099.

De Rosa, M., Esposito, E., Gambacorta, A., Nicolaus, B., Bu'Lock, J.D., 1980. Effects of temperature on ether lipid composition of *Caldariella acidophila*. Phytochemistry, 19(5): 827-831.

Elling, F.J., Könneke, M., Mußmann, M., Greve, A., Hinrichs, K.-U., 2015. Influence of temperature, pH, and salinity on membrane lipid composition and TEX_{86} of marine planktonic thaumarchaeal isolates. Geochimica et Cosmochimica Acta, 171: 238-255.

Elling, F.J. et al., 2017. Chemotaxonomic characterisation of the thaumarchaeal lipidome. Environmental Microbiology, 19(7): 2681-2700.

Fietz, S., Huguet, C., Rueda, G., Hambach, B., Rosell-Melé, A., 2013. Hydroxylated isoprenoidal GDGTs in the Nordic Seas. Marine Chemistry, 152: 1-10.

Herber, J. et al., 2020. A single *Thaumarchaeon* drives nitrification in deep oligotrophic Lake Constance. Environmental Microbiology, 22(1): 212-228.

Hiraoka, S. et al., 2019. Metaepigenomic analysis reveals the unexplored diversity of DNA methylation in an environmental prokaryotic community. Nature Communications, 10(1): 159.

Hopmans, E.C. et al., 2004. A novel proxy for terrestrial organic matter in sediments based on branched and isoprenoid tetraether lipids. Earth and Planetary Science Letters, 224(1–2): 107-116.

Huguet, C., Fietz, S., Rosell-Mele, A., 2013. Global distribution patterns of hydroxy glycerol dialkyl glycerol tetraethers. Organic Geochemistry, 57: 107-118.

Huguet, C., Fietz, S., Rosell-Melé, A., Daura, X., Costenaro, L., 2017. Molecular dynamics simulation study of the effect of glycerol dialkyl glycerol tetraether hydroxylation on membrane thermostability. Biochimica et Biophysica Acta (BBA) - Biomembranes, 1859(5): 966-974.

Huguet, C. et al., 2006. An improved method to determine the absolute abundance of glycerol dibiphytanyl glycerol tetraether lipids. Organic Geochemistry, 37(9): 1036-1041.

Kaiser, J. et al., 2015. Isoprenoid and branched GDGT-based proxies for surface sediments from marine, fjord and lake environments in Chile. Organic Geochemistry, 89: 117-127.

Klotz, F. et al., 2022. Quantification of archaea-driven freshwater nitrification from single cell to ecosystem levels. The ISME Journal.

Könneke, M. et al., 2005. Isolation of an autotrophic ammonia-oxidizing marine archaeon. Nature, 437: 543.

Kou, Q. et al., 2020. Spatial distribution of *n*-alkanes in surface sediments of Selin Co Lake, central Tibetan Plateau, China. Journal of Paleolimnology, 65: 53-67.

Kou, Q. et al., 2022. Distribution, potential sources, and response to water depth of archaeal tetraethers in Tibetan Plateau lake sediments. Chemical Geology, 601: 120825.

Li, J., Lv, L., Wang, R., Long, H., Yang, X., 2022. Spatial distribution of *n*-alkanes in the catchment and sediments of Lake Lugu, Southwest China: Implications for palaeoenvironment reconstruction. Palaeogeography, Palaeoclimatology, Palaeoecology, 592: 110895.

Li, J. et al., 2019. Multiple environmental and ecological controls on archaeal ether lipid distributions in saline ponds. Chemical Geology, 529.

Li, J. et al., 2016. Distribution of glycerol dialkyl glycerol tetraether (GDGT) lipids in a hypersaline lake system. Organic Geochemistry, 99: 113-124.

Li, S.-P., Hu, Y.-Q., Ferguson, D.K., Yao, J.-X., Li, C.-S., 2013. Pollen dispersal in a mountainous area based on pollen analysis of four natural trap types from Lugu Lake, southwest China. Journal of Systematics and Evolution, 51(4): 413-425.

Lin, Q., Liu, E., Zhang, E., Li, K., Shen, J., 2016. Spatial distribution, contamination and ecological risk assessment of heavy metals in surface sediments of Erhai Lake, a large eutrophic plateau lake in southwest China. Catena, 145: 193-203.

Lin, Q. et al., 2018. Reconstruction of atmospheric trace metals pollution in Southwest China using sediments from a large and deep alpine lake: historical trends, sources and sediment focusing. Science of The Total Environment, 613-614: 331-341.

Lin, Y.-S., Mei-liang, Z., Qin, J.-m., 2000. Preliminary study on the characteristics of karst caves and the genesis of Lugu Lake, Yunnan (In Chinese with English abstract). Carsologica Sinica, 19(3): 232-238.

Liu, X.-L. et al., 2012. Mono- and dihydroxyl glycerol dibiphytanyl glycerol tetraethers in marine sediments: identification of both core and intact polar lipid forms. Geochimica et Cosmochimica Acta, 89: 102-115.

Lü, X. et al., 2015. Hydroxylated isoprenoid GDGTs in Chinese coastal seas and their potential as a paleotemperature proxy for mid-to-low latitude marginal seas. Organic Geochemistry, 89: 31-43.

Morrissey, A., Scholz, C.A., Russell, J.M., 2018. Late Quaternary TEX_{86} paleotemperatures from the world's largest desert lake, Lake Turkana, Kenya. Journal of Paleolimnology, 59(1): 103-117.

NIGLAS, 2019. Nanjing Institue of Geography and Limnology Chinese Academy of Sciences (NIGLAS). Investigation of Chinese lakes (in Chinese). Beijing: Science Press, 672 pp.

Pancost, R.D., Hopmans, E.C., Sinninghe Damsté, J.S., 2001. Archaeal lipids in Mediterranean cold seeps: molecular proxies for anaerobic methane oxidation. Geochimica et Cosmochimica Acta, 65(10): 1611-1627.

Park, E. et al., 2019. Seasonality of archaeal lipid flux and GDGT-based thermometry in sinking particles of high-latitude oceans: Fram Strait (79°N) and Antarctic Polar Front (50°S). Biogeosciences, 16(11): 2247-2268.

Podowski, J.C., Paver, S.F., Newton, R.J., Coleman, M.L., 2022. Genome Streamlining, Proteorhodopsin, and Organic Nitrogen Metabolism in Freshwater Nitrifiers. mBio, 13(3): e0237921.

Powers, L.A. et al., 2011. Organic geochemical records of environmental variability in Lake Malawi during the last 700 years, Part I: The TEX_{86} temperature record. Palaeogeography, Palaeoclimatology, Palaeoecology, 303(1-4): 133-139.

Powers, L.A. et al., 2010. Applicability and calibration of the TEX_{86} paleothermometer in lakes. Organic Geochemistry, 41(4): 404-413.

Qin, W. et al., 2017. Influence of oxygen availability on the activities of ammonia-oxidizing archaea. Environmental Microbiology Reports, 9(3): 250-256.

Ren, M., Wang, J., 2022. Phylogenetic divergence and adaptation of *Nitrososphaeria* across lake depths and freshwater ecosystems. The ISME Journal.

Rinke, C. et al., 2021. A standardized archaeal taxonomy for the Genome Taxonomy Database. Nature Microbiology, 6(7): 946-959.

Sarkar, S. et al., 2014. Spatial heterogeneity in lipid biomarker distributions in the catchment and sediments of a crater lake in central India. Organic Geochemistry, 66: 125-136.

Schouten, S., Hopmans, E.C., Schefuß, E., Sinninghe Damsté, J.S., 2002. Distributional variations in marine crenarchaeotal membrane lipids: a new tool for reconstructing ancient sea water temperatures? Earth and Planetary Science Letters, 204(1–2): 265-274.

Schouten, S., Hopmans, E.C., Sinninghe Damsté, J.S., 2013. The organic geochemistry of glycerol dialkyl glycerol tetraether lipids: a review. Organic Geochemistry, 54: 19-61.

Sheng, E. et al., 2015. Late Holocene Indian summer monsoon precipitation history at Lake Lugu, northwestern Yunnan Province, southwestern China. Palaeogeography, Palaeoclimatology, Palaeoecology, 438: 24-33.

Sinninghe Damsté, J.S., Ossebaar, J., Schouten, S., Verschuren, D., 2012. Distribution of tetraether lipids in the 25-ka sedimentary record of Lake Challa: extracting reliable TEX_{86} and MBT/CBT palaeotemperatures from an equatorial African lake. Quaternary Science Reviews, 50: 43-54.

Sinninghe Damsté, J.S. et al., 2018. The enigmatic structure of the crenarchaeol isomer. Organic Geochemistry, 124: 22-28.

Sinninghe Damsté, J.S., Schouten, S., Hopmans, E.C., van Duin, A.C., Geenevasen, J.A., 2002. Crenarchaeol: the characteristic core glycerol dibiphytanyl glycerol tetraether membrane lipid of cosmopolitan pelagic crenarchaeota. Journal of Lipid Research, 43(10): 1641-1651.

Sinninghe Damsté, J.S., Weber, Y., Zopfi, J., Lehmann, M.F., Niemann, H., 2022. Distributions and sources of isoprenoidal GDGTs in Lake Lugano and other central European (peri-)alpine lakes:

635 Lessons for their use as paleotemperature proxies. Quaternary Science Reviews, 277: 107352.
636 Sun, W. et al., 2020. Archaeal lipid-inferred paleohydrology and paleotemperature of Lake Chenghai
637 during the Pleistocene–Holocene transition. Clim of the Past, 16(3): 833-845.
638 Tan, Z., Dong, Y., 2011. Current status of aquatic vegetation in Lugu Lake (In Chinese with English
639 abstract). Environmental Science Survey, 30(6): 26-32.
640 Tierney, J.E. et al., 2010a. Late-twentieth-century warming in Lake Tanganyika unprecedented since AD
641 500. Nature Geoscience, 3(6): 422-425.
642 Tierney, J.E. et al., 2010b. Environmental controls on branched tetraether lipid distributions in tropical
643 East African lake sediments. Geochimica et Cosmochimica Acta, 74(17): 4902-4918.
644 Wang, H., Dong, H., Zhang, C., Jiang, H., Liu, W., 2016. A 12-kyr record of microbial branched and
645 isoprenoid tetraether index in Lake Qinghai, northeastern Qinghai-Tibet Plateau: Implications
646 for paleoclimate reconstruction. Science China Earth Sciences, 59(5): 951-960.
647 Wang, H. et al., 2015. Deglacial and Holocene archaeal lipid-inferred paleohydrology and
648 paleotemperature history of Lake Qinghai, northeastern Qinghai–Tibetan Plateau. Quaternary
649 Research, 83(1): 116-126.
650 Wang, H. et al., 2014a. Water depth affecting thaumarchaeol production in Lake Qinghai, northeastern
651 Qinghai–Tibetan plateau: Implications for paleo lake levels and paleoclimate. Chemical
652 Geology, 368: 76-84.
653 Wang, H. et al., 2019. Lake water depth controlling archaeal tetraether distributions in Midlatitude Asia:
654 implications for paleo lake-level reconstruction. Geophysical Research Letters, 46(10): 5274-
655 5283.
656 Wang, H., Leng, Q., Liu, W., Yang, H., 2017. A rapid lake-shallowing event terminated preservation of
657 the Miocene Clarkia Fossil *Konservat-Lagerstätte* (Idaho, USA). Geology, 45(3): 239-242.
658 Wang, H. et al., 2012a. Distribution of glycerol dialkyl glycerol tetraethers in surface sediments of Lake
659 Qinghai and surrounding soil. Organic Geochemistry, 47: 78-87.
660 Wang, Q., Yang, X., Anderson, N.J., Zhang, E., Li, Y., 2014b. Diatom response to climate forcing of a
661 deep, alpine lake (Lugu Hu, Yunnan, SW China) during the Last Glacial Maximum and its
662 implications for understanding regional monsoon variability. Quaternary Science Reviews, 86:
663 1-12.
664 Wang, Q., Yang, X., Kattel, G.R., 2018. Within-lake spatio-temporal dynamics of cladoceran and diatom
665 communities in a deep subtropical mountain lake (Lugu Lake) in southwest China.
666 Hydrobiologia, 820: 91-113.
667 Wang, S., Dou, H., 1998. Memoirs of Lakes in China (in Chinese). Beijing: Science Press.
668 Wang, Y., Zhu, L., Wang, J., Ju, J., Lin, X., 2012b. The spatial distribution and sedimentary processes of
669 organic matter in surface sediments of Nam Co, Central Tibetan Plateau. Chinese Science
670 Bulletin, 57(36): 4753-4764.
671 Wen, X., 2017. Study on thermodynamics and stable isotopes of water body in the Lugu Lake
672 Dissertation for Doctoral Degree Yunnan Normal University (in Chinese with English abstract).
673 Wu, D. et al., 2020. Temperature-induced dry climate in basins in the northeastern Tibetan Plateau during
674 the early to middle Holocene. Quaternary Science Reviews, 237: 106311.
675 Wuchter, C. et al., 2006. Archaeal nitrification in the ocean. Proceedings of the National Academy of
676 Sciences, 103(33): 12317-12322.

Xie, S. et al., 2012. Microbial lipid records of highly alkaline deposits and enhanced aridity associated with significant uplift of the Tibetan Plateau in the Late Miocene. Geology, 40(4): 291-294.

Yang, H. et al., 2015. The 6-methyl branched tetraethers significantly affect the performance of the methylation index (MBT′) in soils from an altitudinal transect at Mount Shennongjia. Organic Geochemistry, 82: 42-53.

Yang, H. et al., 2019. Depth-dependent variation of archaeal ether lipids along soil and peat profiles from southern China: Implications for the use of isoprenoidal GDGTs as environmental tracers. Organic Geochemistry, 128: 42-56.

Yang, L., 1984. The preliminary study on the original classification and distribution law of lakes on the Yunnan Plateau (in Chinese with English abstract). Transactions of Oceanology & Limnology(1): 34-39.

Yang, Y. et al., 2018. Assessing hydroxylated isoprenoid GDGTs as a paleothermometer for the tropical South China Sea. Organic Geochemistry, 115(Supplement C): 156-165.

Yao, Y., Zhao, J., Bauersachs, T., Huang, Y., 2019. Effect of water depth on the TEX_{86} proxy in volcanic lakes of northeastern China. Organic Geochemistry, 129: 88-98.

Yu, Z.T., Wang, X.J., Zhang, E.L., Zhao, C.Y., Liu, X.Q., 2015. Spatial distribution and sources of organic carbon in the surface sediment of Bosten Lake, China. Biogeosciences, 12(22): 6605-6615.

Zhang, E. et al., 2013. Within-lake variability of subfossil chironomid assemblage in a large, deep subtropical lake (Lugu lake, southwest China). Journal of Limnology, 72(1): 117-126.

Zhang, E., Sun, W., Chang, J., Ning, D., Shulmeister, J., 2018. Variations of the Indian summer monsoon over the last 30 000 years inferred from a pyrogenic carbon record from south-west China. Journal of Quaternary Science, 33(1): 131-138.

Zhang, S., Xie, X., Wan, G., 1997. Mineralogical records and their environmental aspects of Lugu Lake, Yunnan Province (In Chinese with English abstract). Acta Mineralogica Sinica, 17(2): 183-193.

Zhang, Y., Pagani, M., Wang, Z., 2016. Ring Index: A new strategy to evaluate the integrity of TEX_{86} paleothermometry. Paleoceanography, 31(2): 220-232.

Zhang, Y. et al., 2011. Methane Index: A tetraether archaeal lipid biomarker indicator for detecting the instability of marine gas hydrates. Earth and Planetary Science Letters, 307(3–4): 525-534.

Zhao, H., Kong, D., Fan, Y., Tan, Z., 2016. Current status of aquatic marcrophyte and analysis of its variation in lakeside zone of Luguhu Lake (In Chinese with English abstract). Environmental Science Survey, 35(03): 48-53.

Figure Captions

Fig. 1. Bathymetry of Lake Lugu and sampling sites. Surface sediments (n = 54) from different water depths and topsoils (n = 9) from the catchment of Lake Lugu were collected. The light blue dots indicate samples collected at the water depth < 20 m (n = 14). The dark blue dots represent samples collected at the water depth > 20 m (n = 40). The yellow triangles indicate soils collected in the catchment of Lake Lugu.

Fig. 2. (a) Average distribution of isoGDGTs in surface sediments and surrounding soils within the catchment of Lake Lugu. (b) Average distribution of OH-GDGTs in surface sediments. (c) Principal component analysis (PCA) on the distribution of iso GDGTs from surface sediments and surrounding soils. (d) Redundancy analysis (RDA) on the distribution of isoGDGTs from surface sediments and surrounding soils. (e) PCA biplot of OH-GDGTs in surface sediments. (f) RDA triplot of OH-GDGTs in surface sediments. The light blue dots indicate samples collected at the water depth < 20 m (n = 14). The dark blue dots represent samples collected at the water depth > 20 m (n = 40). The yellow triangles indicate soils collected in the catchment of Lake Lugu.

Fig. 3. Boxplots of the concentration of crenarchaeol (a); TEX_{86} (b); BIT(c); RI(d); GDGT-0/Cren(e); GDGT-2/GDGT-3(f); Cren/Cren'(g) in the surface sediments and surrounding soils. (h) Boxplot of %OH-GDGTs in the surface sediments. Shallow sediments indicate samples collected at the water depth < 20 m (n = 14). Deep sediments represent samples collected at the water depth > 20 m (n = 40).

Fig. 4. Cross plots of %GDGT-0 (a), %Cren (b), BIT (c), and %OH-GDGTs (d) in surface sediments versus water depth. Cross plots of the concentrations of GDGT-0 and crenarchaeol (e), summed OH-GDGTs and isoGDGTs (f), summed OH-GDGTs and GDGT-0 (g), and summed OH-GDGTs and crenarchaeol (h) in the surface sediments. The light blue triangles indicate samples collected at the water depth < 20 m. The dark blue dots represent samples collected at the water depth > 20 m. The linear regression of shallow sediment (< 20 m) is indicated in light blue. The linear regression of deep sediment (> 20 m) is indicated in dark blue. The black linear regression represents for all sediment samples (n = 54).

Fig. 5. Spatial distribution of %Cren (a), %OH-GDGTs (b), Cren/Cren' (c), and BIT

(d) in the surface sediments of Lake Lugu.

Fig. 6. Cross plots of %Cren (a), %OH-GDGTs (b), Cren/Cren' (c), and BIT (d) in surface sediments versus water depth. The dark grey dots indicate samples in this study. The light grey dots include lake samples from this study, midlatitude Asia (Wang et al., 2019) and Tibetan Plateau (Kou et al., 2022).

Fig. 1.

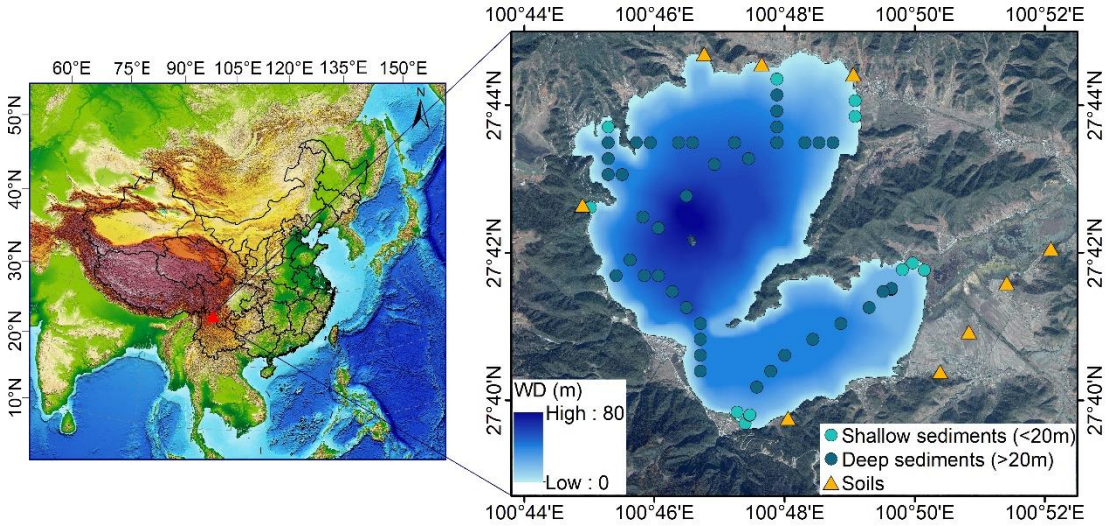
60°E
75°E
90°E
105°E
120°E
135°E
150°E
50°N
40°N
30°N
20°N
10°N
N
100°44'E
100°46'E
100°48'E
100°50'E
100°52'E
27°44'N
27°42'N
27°40'N
WD (m)
High : 80
Low : 0
Shallow sediments (<20m)
Deep sediments (>20m)
Soils

Fig. 2.

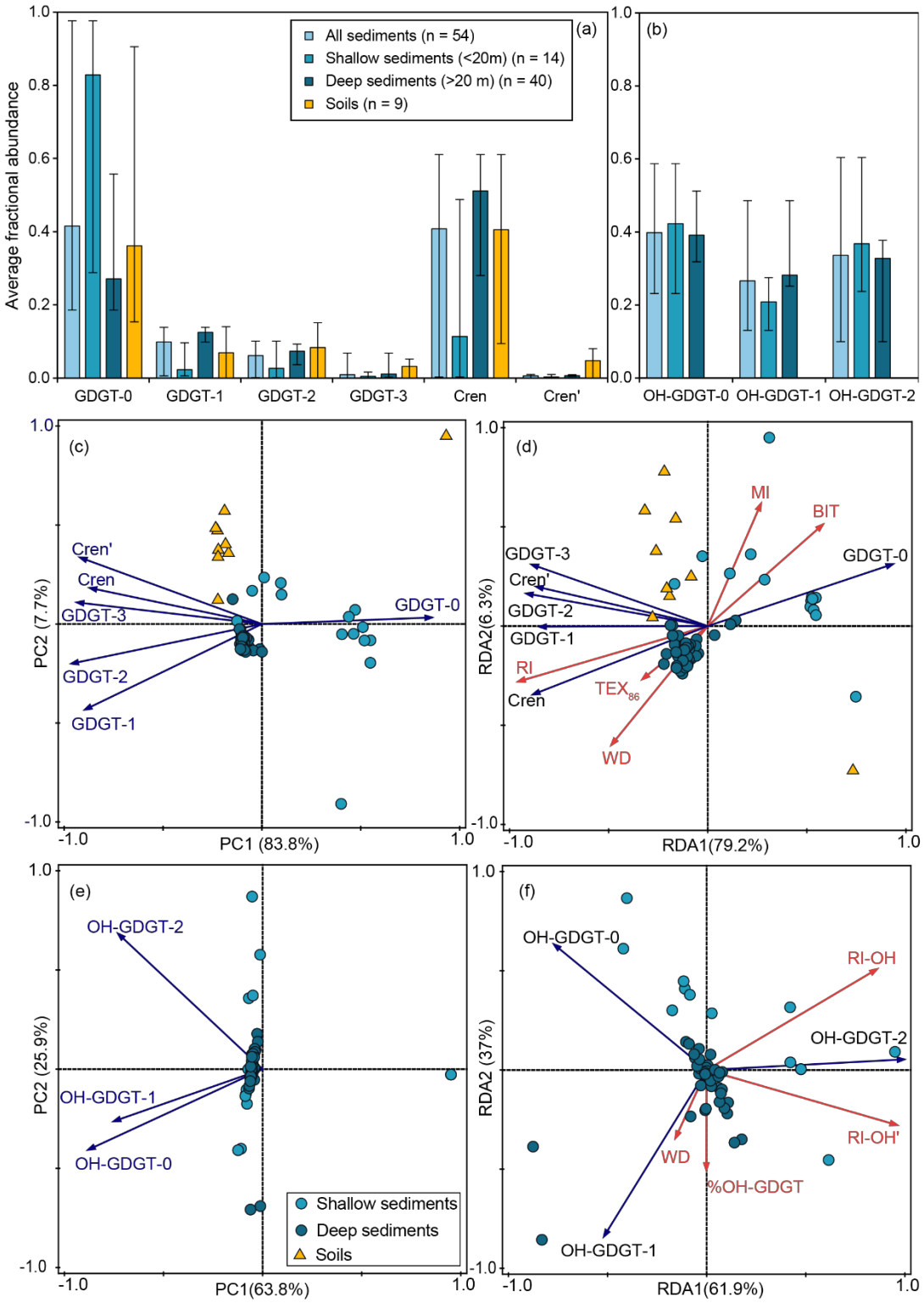
(a)
All sediments (n = 54)
Shallow sediments (<20m) (n = 14)
Deep sediments (>20 m) (n = 40)
Soils (n = 9)
Average fractional abundance
GDGT-0
GDGT-1
GDGT-2
GDGT-3
Cren
Cren'
(b)
OH-GDGT-0
OH-GDGT-1
OH-GDGT-2
(c)
PC2 (7.7%)
PC1 (83.8%)
(d)
RDA2(6.3%)
RDA1(79.2%)
MI
BIT
RI
TEX86
WD
(e)
PC2 (25.9%)
PC1(63.8%)
Shallow sediments
Deep sediments
Soils
(f)
RDA2 (37%)
RDA1(61.9%)
RI-OH
RI-OH'
%OH-GDGT

Fig. 3.

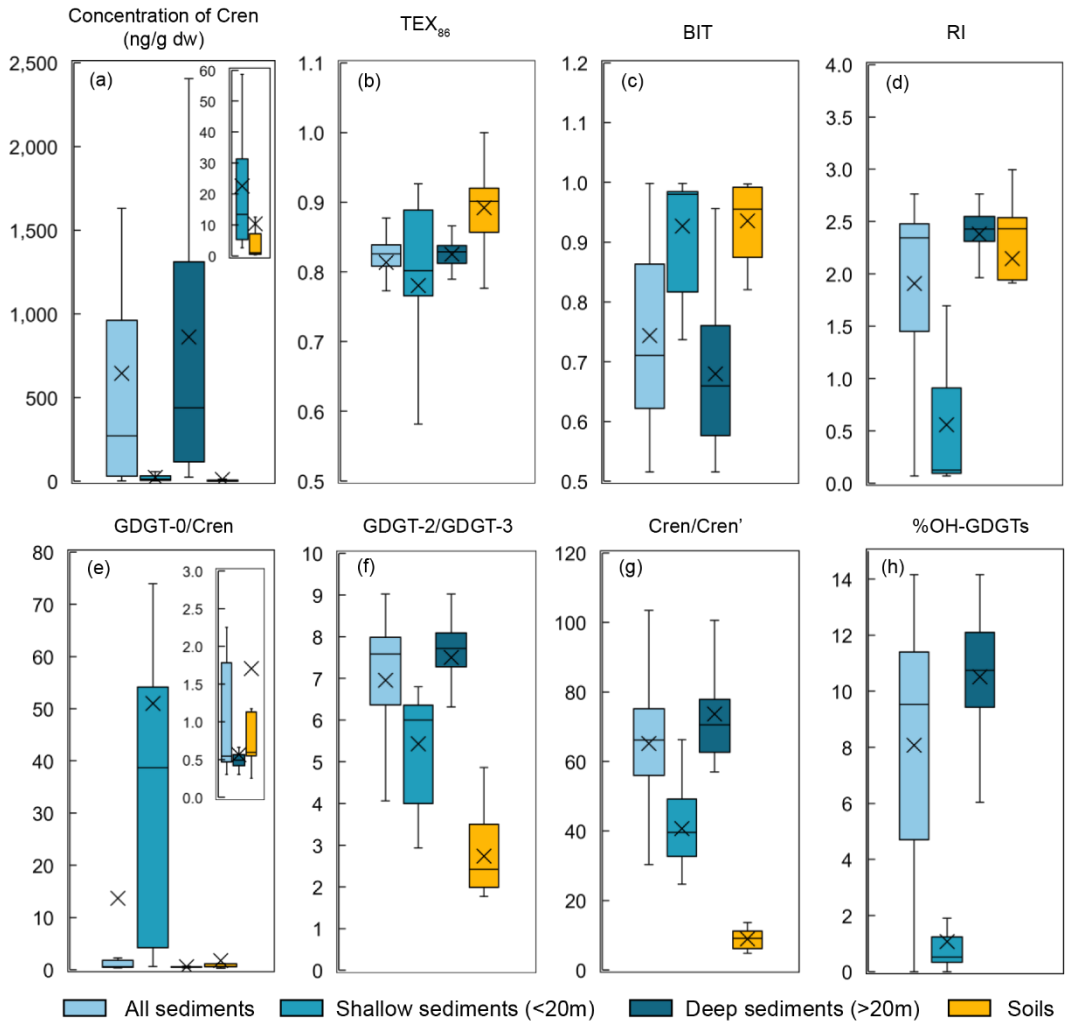
Concentration of Cren (ng/g dw)
TEX86
BIT
RI
(a)
(b)
(c)
(d)
GDGT-0/Cren
GDGT-2/GDGT-3
Cren/Cren'
%OH-GDGTs
(e)
(f)
(g)
(h)
All sediments
Shallow sediments (<20m)
Deep sediments (>20m)
Soils

Fig. 4.

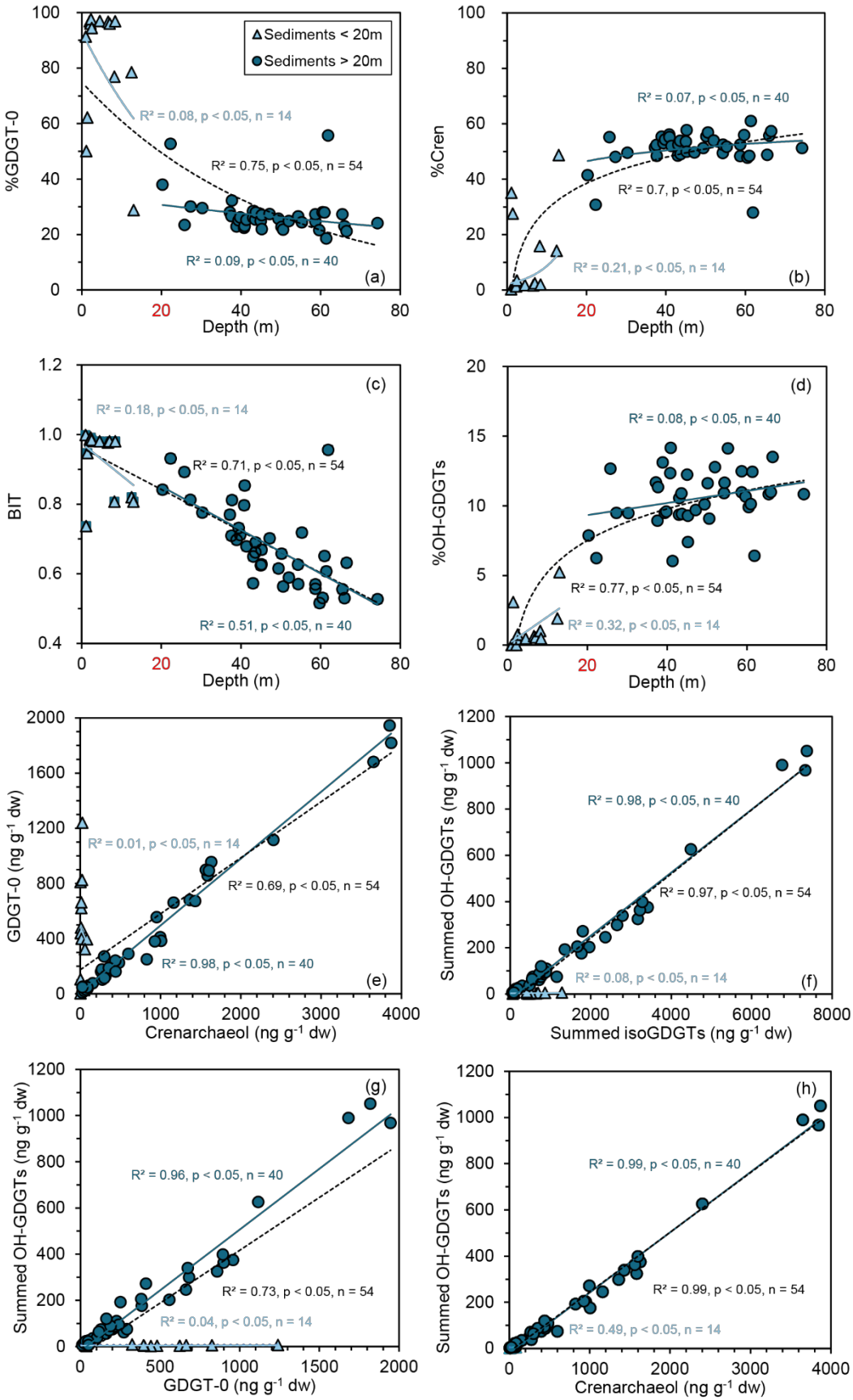
Sediments < 20m
Sediments > 20m
%GDGT-0
Depth (m)
R² = 0.08, p < 0.05, n = 14
R² = 0.75, p < 0.05, n = 54
R² = 0.09, p < 0.05, n = 40
(a)
%Cren
R² = 0.07, p < 0.05, n = 40
R² = 0.7, p < 0.05, n = 54
R² = 0.21, p < 0.05, n = 14
(b)
BIT
R² = 0.18, p < 0.05, n = 14
R² = 0.71, p < 0.05, n = 54
R² = 0.51, p < 0.05, n = 40
(c)
%OH-GDGTs
R² = 0.08, p < 0.05, n = 40
R² = 0.77, p < 0.05, n = 54
R² = 0.32, p < 0.05, n = 14
(d)
GDGT-0 (ng g-1 dw)
Crenarchaeol (ng g-1 dw)
R² = 0.01, p < 0.05, n = 14
R² = 0.69, p < 0.05, n = 54
R² = 0.98, p < 0.05, n = 40
(e)
Summed OH-GDGTs (ng g-1 dw)
Summed isoGDGTs (ng g-1 dw)
R² = 0.98, p < 0.05, n = 40
R² = 0.97, p < 0.05, n = 54
R² = 0.08, p < 0.05, n = 14
(f)
R² = 0.96, p < 0.05, n = 40
R² = 0.73, p < 0.05, n = 54
R² = 0.04, p < 0.05, n = 14
(g)
GDGT-0 (ng g-1 dw)
R² = 0.99, p < 0.05, n = 40
R² = 0.99, p < 0.05, n = 54
R² = 0.49, p < 0.05, n = 14
(h)

Fig. 5

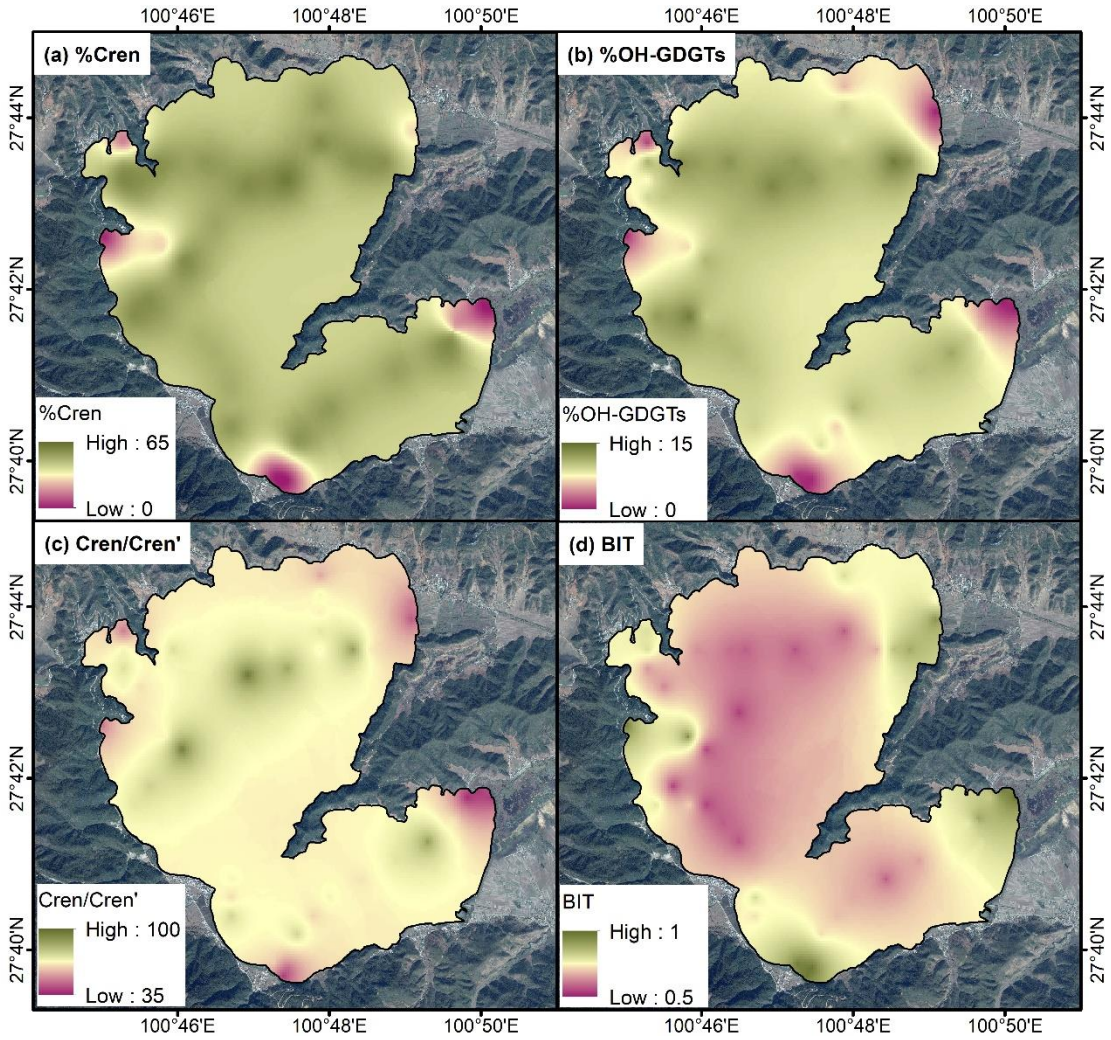
(a) %Cren
%Cren
High : 65
Low : 0
(b) %OH-GDGTs
%OH-GDGTs
High : 15
Low : 0
(c) Cren/Cren'
Cren/Cren'
High : 100
Low : 35
(d) BIT
BIT
High : 1
Low : 0.5
100°46'E
100°48'E
100°50'E
27°44'N
27°42'N
27°40'N

Fig. 6

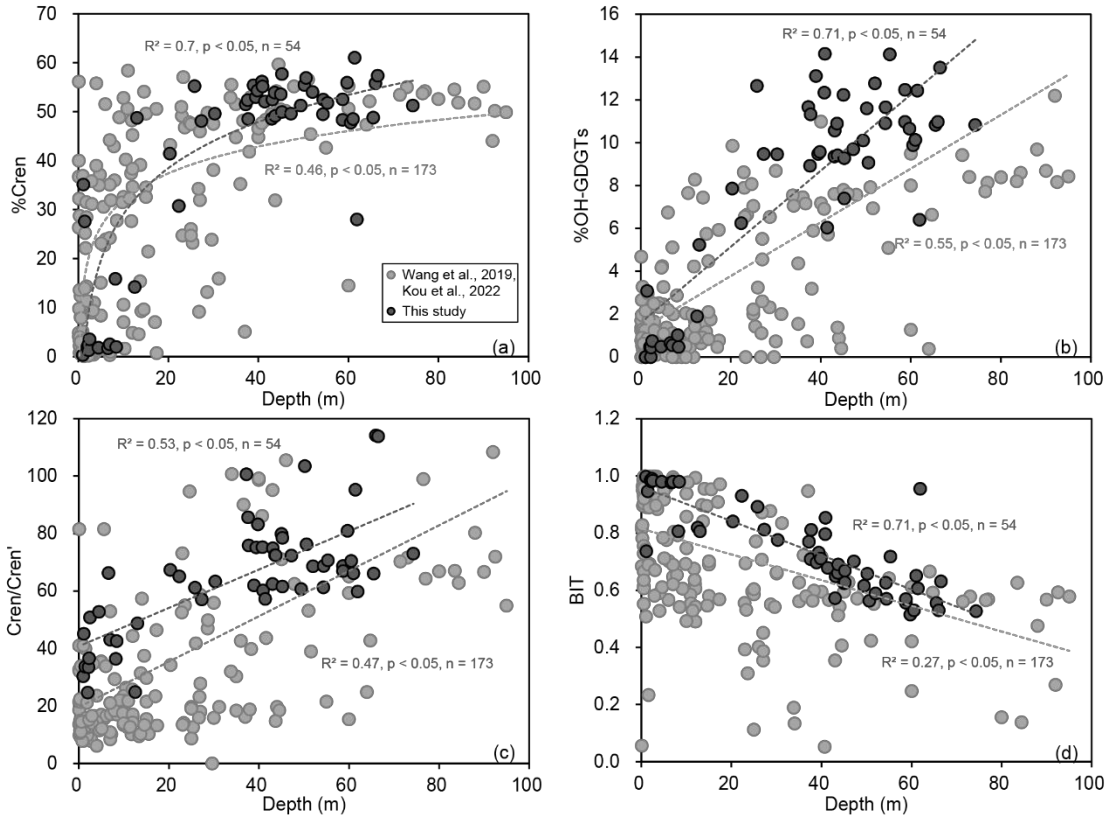
R² = 0.7, p < 0.05, n = 54
R² = 0.46, p < 0.05, n = 173
Wang et al., 2019, Kou et al., 2022
This study
%Cren
Depth (m)
(a)
R² = 0.71, p < 0.05, n = 54
R² = 0.55, p < 0.05, n = 173
%OH-GDGTs
Depth (m)
(b)
R² = 0.53, p < 0.05, n = 54
R² = 0.47, p < 0.05, n = 173
Cren/Cren'
Depth (m)
(c)
R² = 0.71, p < 0.05, n = 54
R² = 0.27, p < 0.05, n = 173
BIT
Depth (m)
(d)